◆ Human Brain Mapping 8:259–271(1999) ◆

Temporal Properties of the Hemodynamic Response in Functional MRI

F. Kruggel* and D.Y. von Cramon

Max-Planck-Institute of Cognitive Neuroscience, Leipzig, Germany

Abstract: Today, most studies of cognitive processes using functional magnetic resonance imaging (fMRI) adopt an event-related experimental design. Highly flexible stimulation settings require new statistical models where not only the activation amount, but also the time course of the measured hemodynamic response is analyzed. It is possible to obtain statistically valid descriptions of single hemodynamic responses from a robust nonlinear estimation procedure. Focus is placed on the temporal behaviour of the hemodynamic response: relative temporal order, changes induced by modification of the experimental context, and interindividual differences. Example analyses from recent fMRI studies underline the usefulness of this approach. *Hum. Brain Mapping 8:259–271, 1999.*

Key words: fMRI; event-related design; hemodynamic response; temporal analysis

INTRODUCTION

The metabolic processes involved in neuronal activation consume oxygen [Vilringer and Dirnagl, 1995; Gjedde, 1997]. A locally diminished oxygen tension induces a dilation of arterioles, followed by an increased blood inflow and, finally, an oversupply of oxygenated hemoglobin in the capillary and venous compartment. This effect is called the hemodynamic response (HR). The mechanisms of the neurono-vascular coupling are still under investigation. Stimulus-induced changes in the local concentration of deoxy-hemoglobin can be most easily measured today as a dephasing effect in T_2^*-weighted magnetic resonance images. This blood-oxygen-level-dependent (BOLD) contrast [Belliveau et al., 1991; Kwong et al., 1992, Ogawa et al., 1992] is now the most popular method in functional magnetic resonance imaging (fMRI) and is employed as one of the major experimental methods for analyzing cognitive processes in humans.

Understanding brain function requires information not only on the spatial localization of neural activity, but also on its temporal evolution. There is an increasing interest in the time course (i.e., the shape) of the HR and its modulation with respect to different experimental conditions. So the question is raised to what extent conclusions may be drawn about the neuronal event from the HR shape. However, vascular processes take time at least an order longer than the underlying functional activation: the time-to-maximum of a HR due to a transient stimulus is typically delayed by 5–8 sec and dispersed by 3–4 sec [Friston et al., 1994a; Sorensen et al., 1996]. The key to detecting changes in the temporal properties with a higher resolution than 2 sec is the adoption and deconvolution of the HR by a model function [Kim et al., 1997].

There is no consensus about a physiological model for the neurono-vascular coupling that would allow one to derive a spatio-temporal model function for the HR. However, a number of heuristic models [Friston et

*Correspondence to: Frithjof Kruggel, Max-Planck-Institute of Cognitive Neuroscience, Stephanstraβe 1, D-04103 Leipzig, Germany. Email: kruggel@cns.mpg.de

Received for publication 16 October 1998; accepted 18 June 1999

al., 1994a; Cohen, 1997; Lange and Zeger, 1997; Friston et al., 1998a; Rajapakse et al., 1998] were based on the idea of describing a HR by a linear convolution of the neuronal activation with a hemodynamic modulation function. The primary objective for this work was to achieve a higher specifity in the detection of functional activation in the presence of a high noise level. The evolution of these models follow their complexity: early models assume constant preset values for the lag [Friston et al., 1994a], whereas current models determine HR parameters like lag and dispersion voxelwise from the data [Cohen, 1997; Lange and Zeger, 1997; Rajapakse et al., 1998]. Differences in HR parameters at different sites and between subjects were described [Rajapakse et al., 1998] and underline the usefulness of this approach.

One of the reasons for site-dependent differences in HR parameters is found with the local tissue composition. It has long been under debate which tissue compartment dominates the signal measured in fMRI. Because in a tissue of average composition, 70% are comprised of venules and veins, it was argued that $>$90% of the signal originates in the venous compartment [Gjedde, 1997]. Since the draining veins could be located close to, or at some distance from, the capillary compartment, the appearance of a strong signal from the veins could make it difficult to pinpoint the (cortical) location where the activation occurred. This is known as the ''brain vs. vein'' debate [Singh et al., 1995]. This issue was partly resolved by examining the temporal properties of the HR: as known for years in cerebral angiography, there is a delay of 3–4 sec in the transition of a contrast agent from the cortical compartment to the early venous phase [Piepgras, 1977]. This was confirmed by reports of a bimodal temporal distribution in fMRI: a phase shift corresponding to a time delay of 5.5 sec was noted for the HR of cortical areas vs. veins [Lee et al., 1995; Singh et al., 1995].

By careful modification of the experimental context from trial to trial, relative changes of the HR shape may be induced. This technique is known as event-related fMRI [Buckner et al., 1996; Josephs et al., 1997; Zarahn et al., 1997], and very recently, reports about HR shape changes due to changes in the stimulation context appeared in the literature. In a study of episodic memory, a temporal shift of activation centers was described in conjunction with an experimental delay time variation of 2–6 sec [Buckner et al., 1998b]. Friston and colleagues [1998b] discuss that ''in some instances fMRI can discriminate between dynamics on a 100 msec timescale despite relatively long repetition times.'' However, no report about lag times and their variability are included here. Luknowsky et al. [1998] studied the lag times of the V1 and M1 areas in a visuo-motor reaction task using shifts in a hemifield stimulation. A high correlation between the presentation delay and the HR lag was found, as well as a high correlation between the V1-M1 time difference and the reaction times.

In the context of an event-related fMRI experiment, it is useful to describe the observed HR trial- and region-specific by a set of parsimonious parameters. Variations of these parameters with the experimental context may allow the drawing of more detailed conclusions about the amount and time course of neuronal activation underlying the HR. Recently, we described and validated a nonlinear regression context to allow such analyses [Kruggel and von Cramon, 1999]. In this study, we compile results and experiences obtained with a nonlinear regression context in a number of different event-related experiments. We focus on the temporal behaviour of the HR: the relative order in which HR arise, changes induced by modifying the experimental context, and differences between subjects. In the next section, we formally describe the analytical procedure. Then, we report results obtained by this procedure: general properties of the HR, an example case study from a language experiment, and a group analysis of an experiment in working memory function.

PARAMETER ESTIMATION

We adapted a model function to the hemodynamic response and generated parameter sets for each trial and each predefined region-of-interest (ROI). This section describes the data preprocessing steps and the estimation context by which results in this study were obtained.

Preprocessing

The objective of preprocessing fMRI data is to separate the functional activation from artifacts induced by the scanning process, physiological noise (i.e., breathing, motion, pulsations), and to correct for baseline fluctuations. All data sets included in this study were preprocessed by the following steps [Kruggel et al., 1998a]: (1) removal of trials contaminated by gross artifacts, (2) correction for in-plane movements, (3) baseline correction by subtraction of a low pass-filtered signal in the temporal domain (using a cutoff frequency of 1.5 times the trial length), (4) noise filtering in the temporal domain (using a cutoff frequency of 0.4 times the trial length). Steps (3) and (4) include the fundamental frequency (corresponding to

the stimulation) and its first harmonic in the passband. Temporal correlations enhanced by filtering are accounted for in the statistical model (see below).

Definition of regions-of-interest

Because we focused on the temporal aspects of the HR in this study, we defined ROIs that are assumed to be stationary in space. In principle, any method for defining such regions may be applied. Because the size of a region influences the variance of the parameter estimations, regions should not be too small. In our experiments, we found an optimal region size of 60 − 90 mm^2 (4–6 voxels).

To achieve a good signal-to-noise ratio, we used a procedure to select automatically the most highly activated voxels in a brain region. We applied standard procedures to detect functional activation in the data: (1) analysis for activated regions by Pearson correlation with a time-shifted box-car waveform ($\Delta = 6$s), (2) conversion of the correlation coefficient into z-scores and thresholding of the corresponding SPM{z} by a score of 8, (3) assessment of the activated regions for their significance on the basis of their spatial extent [Friston et al., 1994b], (4) detection of local maxima in the thresholded SPM{z}, [5] selection of the six most highly activated 4-connected voxels around local maxima in the SPM{z}.

Description of estimation model

Our estimation model has already been described in detail [Kruggel and von Cramon, 1999]. Excellent discussions about nonlinear regression procedures are given in Bates [1988] and Seber and Wild [1989].

HR parameter definition

We model the n-dimensional vector of acquired functional data y, sampled a k voxel sites on l timesteps of a single stimulation period, as a sum of a deterministic function $g(\cdot)$ and a stochastic part ϵ:

$$\mathrm{y} = g(\mathrm{t}, \beta) + \epsilon, \tag{1}$$

where t denotes the time and β the p-dimensional vector of model parameters. The best compromise between goodness-of-fit and the number of model parameters is found with the Gaussian function [Rajapakse et al., 1998]:

$$g(t, \beta) = \frac{\beta_0}{\beta_1\sqrt{2\pi}} \exp\left(-\frac{(t-\beta_2)^2}{2\beta_1^2}\right) + \beta_3 \tag{2}$$

We denote the components of β as β_0: gain (the ''height'' of the HR), β_1: dispersion (proportional to the duration of the HR), β_2: lag (time delay from stimulation onset to HR peak), and β_3: baseline. As an independent measure derived from the data, we define the norm of a HR as the difference between a data point and the baseline, summed over all points and timesteps in a trial: $\Sigma_{i=1}^{n}(y_i - \beta_3)$.

Stochastic background model

It was shown [Bullmore et al., 1996; Benali et al., 1997; Kruggel and von Cramon, 1999] that the stochastic part in preprocessed fMRI data may be described approximately by an Ornstein-Uhlenbeck process [Neumaier and Schneider, 1998]: (1) it is stationary with respect to time, (2) its elements ϵ_i are normally distributed with a covariance matrix V: $\epsilon \sim \mathrm{N}(0, \mathrm{V})$, and (3) their correlation is described by an AR(1) model.

This correlation is determined from the data by fitting an exponential function to the experimentally obtained semivariogram η [Christensen, 1991; Cressie, 1993] in each spatial and in the temporal dimension separately:

$$\eta(h) = \begin{cases} 0 & \text{if} \quad h = 0, \\ \alpha_0(1 - \exp(-\alpha_1 h)) & \text{otherwise,} \end{cases} \tag{3}$$

where h is the distance between two voxel sites, either in time or space. From the model parameters, we can derive the variance $\sigma^2 = \alpha_0$ and the autocorrelation $\rho = \exp(-\alpha_1)$. Then, the (spatial) covariance matrix S of a linear array of k voxels is defined as:

$$\mathrm{S} = \sigma^2 \begin{pmatrix} 1 & \rho & \rho^2 & \cdots & \rho^{k-1} \\ \rho & 1 & \rho & \cdots & \rho^{k-2} \\ \rho^2 & \rho & 1 & \cdots & \rho^{k-3} \\ & & & \cdots & \\ \rho^{k-1} & & & \cdots & 1 \end{pmatrix}, \tag{4}$$

Finally, the spatio-temporal covariance matrix V is given by the tensor product of the spatial and temporal matrices:

$$\mathrm{V} = \mathrm{S}_x \otimes \mathrm{S}_y \otimes \mathrm{T}. \tag{5}$$

Estimation

Having set up our model equations, we find the ML estimate $\hat{\beta}$ of our model parameters as the vector β

that minimizes the quantity:

$$\arg\min_{\beta} \{(y - g(t, \beta))^T V^{-1} (y - g(t, \beta))\}. \quad (6)$$

In the case of the Gaussian function, this problem corresponds to a 4D nonlinear minimization problem, which can be solved by the downhill simplex method of Nelder and Mead [Press et al., 1992].

Since the residuals required to set up the covariance matrix are unknown beforehand, the estimation process is iterative. During the first run, we determine the semivariogram according to Eq. 3 from the data y and during subsequent runs from the residuals. We found five iterations sufficient to stabilize the estimations.

Confidence limits

Using a first-order linear model, we can derive confidence limits for the estimation from the inverse of the Fisher information matrix F [Cox and Ma, 1995; Walter and Ponzatto, 1997]:

$$\hat{\beta} \sim N(\beta, F_\beta^{-1}), \quad \text{where} \quad F_\beta = G_\beta V^{-1} G_\beta^T. \quad (7)$$

and G_β denotes the Jacobian matrix of $g(\cdot)$ with respect to β.

Goodness-of-fit

A simple measure for the goodness-of-fit (GOF) of the model to the data is derived from the residuals $\epsilon = y - g(t, \beta)$ as:

$$GOF = \frac{\epsilon^T V^{-1} \epsilon}{y^T V^{-1} y}, \quad \text{GOF} \in [0, 1], \quad (8)$$

with 0 denoting a perfect fit. A more complex but exact equation for the F-statistics is given by [Hartley, 1964; Seber, 1989, pp. 236–238]:

$$F_{p,n-p} \sim \frac{(n-p)}{p} \frac{\epsilon^T P \epsilon}{\epsilon^T (I_n - P) \epsilon}, \quad \text{using} \quad P = G_\beta F_\beta^{-1} G_\beta^T \quad (9)$$

where n corresponds to the number of data points, p to the number of parameters, and I_n is the (n,n) identity matrix. Both measures may be used to detect trials where the model function does not fit the HR well. The reasons for such misfits and their frequency are discussed later.

RESULTS

To underline the usefulness of HR modeling in the analysis of fMRI data, we report results obtained in three different studies: (1) general findings about relations between the model parameters, (2) an in-depth analysis of a sample fMRI experiment in language comprehension, (3) a group analysis of a fMRI study of working memory. All data sets were obtained using an EPI protocol (single shot, gradient recalled, TE 30 msec, 40° flip angle, TR 1,000 resp., 2,000 msec) on a 3T MR scanner (Bruker Medspec 30/100).

Properties of model parameters

We checked the relations between model parameters in various sites, different fMRI experiments, as well as within and between subjects. We report here on the general findings.

There is a highly significant proportionality between the gain and the dispersion of a hemodynamic response (i.e., the ''height'' and the ''width''), indicating that there is an upper limit for the HR slope. This limit depends on the activation site: primary cortices generally show rather high slopes and are slightly skewed to the left, i.e., the rising flank is steeper. With secondary cortices and basal ganglia, this limit is lower. The HR in venous areas is usually symmetric with slopes similar to primary cortices (see Fig. 1).

No simple dependency between the HR gain and lag is found. First, the slope limit imposes a shift on the HR maximum (i.e., on the lag) for greater activations. Second, the lag depends on the activation site. In the example regions of Figure 1, primary cortices reach their maximum first (mean = 7.37 ± 1.25s), then secondary cortices (mean = 8.61 ± 1.86s), then veins (mean = 10.62 ± 2.32s). Third, lag and norm depend on the stimulation conditions.

In a first approximation, lag and dispersion of a HR are independent. The dispersion is related to the duration of a response and is thus subjected to the stimulus duration.

If the HR fits a Gaussian model well, norm and gain should be proportional. We intended the norm as a measure that is (apart from the baseline parameter) independent of the estimated parameter set and ''closer to the data.'' Thus an inspection of the distribution of the ratio norm/gain should reveal information about trials in which the Gaussian model does not fit well to the HR. For most responses, we found this ratio close to 2.4 (at TR = 2.0s, $p < 1e-12$). Ratios lower than 2.0 corresponded to trials with ''crippled'' responses that

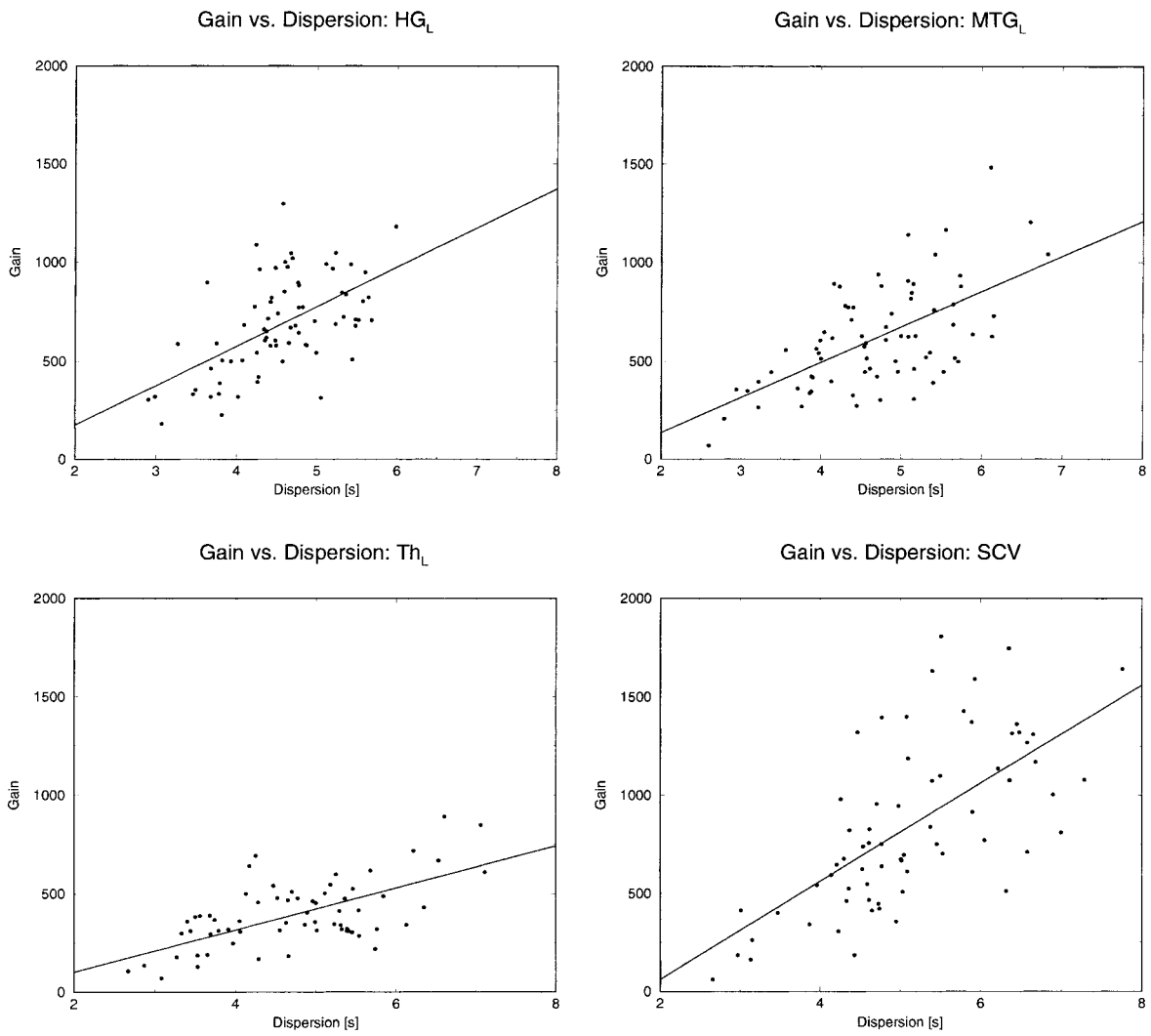

Figure 1.
HR dispersion vs. norm for sample regions: Top left: left Heschl's gyrus ($-225 + 200x$, $R^2 = 0.31$, $p = 1.8e-7$); top right: left medio-temporal gyrus ($-222 + 179x$, $R^2 = 0.37$, $p = 1.1e-8$); bottom left: left thalamus ($-114 + 107x$, $R^2 = 0.48$, $p = 7.2e-11$); bottom right: vein complex ($-439 + 250x$, $R^2 = 0.51$, $p = 3.8e-12$).

were not linked to the stimulus. Ratios above 2.8 were found in trials that were typically overlaid by transient artifacts. Depending on the region of interest and the signal-to-noise level, between 0–15% of the responses were detected as such outliers. Thus if a model fit is ensured by one of the GOF measures, norm and gain may be used interchangably.

Example fMRI analysis

We randomly selected a fMRI dataset from a recent experimental study in language processing [Meyer et al., 1998]. Single sentences were presented aurally, and subjects were asked to classify a sentence grammatically for correctness. The presentation of a sentence needed ~6 sec, followed by a pause of 18 sec. Seventy-six trials were recorded during an ~30 min experiment. During this time, every 4 sec we acquired four slices of 128 × 64 voxel with a spatial resolution of 1.9 × 3.8 × 5 mm and 2 mm gap. For consistency, a single dataset was chosen to demonstrate the use of the procedures discussed here. Similar evaluations have been performed on a large number of datasets and different experimental designs.

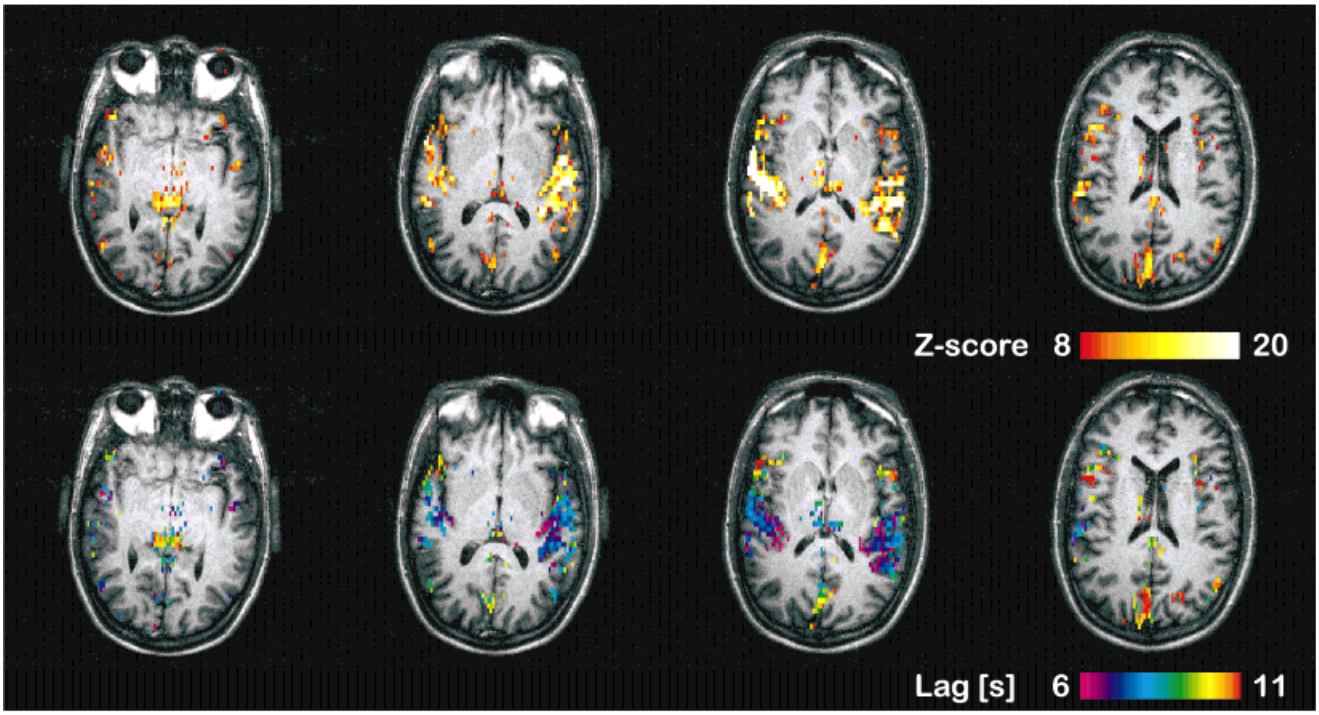

Figure 2.
Top row: significantly activated regions from an experiment in language processing. Bottom row: lag times (in s) for the HR in the activated regions. Magenta-blue areas correspond to early responses, blue-green areas to middle, yellow-red areas to late responses.

Relative temporal ordering

First, the standard procedures to detect functional activity in this dataset were performed (Fig. 2): (1) *preprocessing* using motion correction, baseline estimation, and lowpass-filtering for noise [Kruggel et al., 1998a], (2) *statistical analysis* for activated regions by Pearson correlation with a time-shifted box-car waveform ($\Delta = 6$s) and conversion of the correlation coefficients into z-scores, (3) *assessment of significance* of the activated regions on the basis of their spatial extent [Friston et al., 1994b], using a z-score threshold of 8 (Fig. 2). We can display the lag values in a voxelwise overlay for interpretation in conjunction with a SPM (see lag map in the bottom row of Fig. 2). There is a clear distinction in the lag values for early responses (magenta-blue, ~6–8 sec), middle (blue-green, ~8–10 sec), and late responses (yellow-red, ~10 sec). Note that early responses are found with the auditory cortices, middle responses with secondary, language-related cortices, and late responses with veins. In comparing the upper and lower rows of Figure 2, it is important to note that a single activated region does not necessarily show a consistent temporal behaviour. Of course, this is a consequence of the crude HR modeling by the box-car waveform, which acts as an ''integration over time'' here.

Second, we defined regions of interests (ROIs) by selecting the six most highly activated connected voxels from the z-score map. In the 42 ROIs found, we adapted our HR model in each of the 76 trials, thus yielding 42×76 estimates for the gain, norm, lag, and dispersion. Timings were corrected for the slice acquisition delay in the EPI protocol. To show the relation of lag times in ROIs, we selected a few ROIs at functionally interesting anatomical locations here. Average values and confidence ranges of the norm, lag, and dispersion are compiled in Table I. We have run t-tests (single sided, paired within a trial, unequal variance, $P = 0.05$) on the lag values for single trials and found a temporal ordering of: $HG_L \sim HG_R < MT_R \sim TH_R \sim TH_L < ST_L \sim FO_L \sim PC < SCV$. Note that primary cortical areas arise first, then secondary cortical areas, then veins.

Interestingly, a temporal ordering also can be found along a trajectory starting from the mesial part of Heschl's gyrus, running outward on the superior

temporal gyrus and anteriorly (see Fig. 3). All time differences are significant.

Dependency on experimental context

During the experiment, reaction times and responses were recorded. The presentation length of the sentence varied between 2,560–4,460 msec. We evaluated the influence of the stimulation context on the HR parameters by multivariate linear regression models. From the behavioral data alone, we learned that the reaction time is primarily dependent on the trial number, i.e., there was a training effect. Second, it depended on the sentence length, but not on the correctness manipulation. To compare the HR with the stimulation, we used the sentence length rather than the reaction time.

When evaluating over all ROIs and all trials (n = 2,330), we found that per second of increasing sentence length, the lag increased by 880 msec (±110 msec, p = 3e − 15) and the dispersion by 210 msec (±67 ms, p = 4e − 8) (see Fig. 4). So within this temporal stimulus range, there is a direct proportionality between the stimulus and HR duration. Likewise, the norm increased by 21% per second stimulus duration, indicating that a longer "computation time" demands a higher amount of energy.

TABLE I. Average values and confidence ranges of norm, lag, and dispersion for sample regions of the experiment in Figure 2

Location	Norm	Lag [s]	Dispersion [s]
Sup. temporal gyrus left (ST_L)	1547 ± 741	9.25 ± 2.01	5.01 ± 1.32
Vein complex (SCV[a])	1680 ± 877	10.25 ± 2.36	5.01 ± 1.27
Precuneus (PC)	861 ± 389	9.66 ± 2.30	4.86 ± 1.39
Heschl's gyrus left (HG_L)	1241 ± 934	6.98 ± 1.28	4.66 ± 1.08
Heschl's gyrus right (HG_R)	1353 ± 515	7.30 ± 1.21	4.60 ± 0.93
Medio-temporal gyrus right (MT_R)	1341 ± 576	8.24 ± 2.02	4.77 ± 1.18
Thalamus left (TH_L)	893 ± 451	8.49 ± 1.80	4.97 ± 1.44
Thalamus right (TH_R)	956 ± 395	8.34 ± 1.97	4.96 ± 1.38
Anterior insula left (AI_L)	766 ± 366	9.80 ± 2.97	4.87 ± 1.50
Frontal operculum left (FO_L)	926 ± 402	9.66 ± 2.47	4.85 ± 1.32

[a] In vicinity of the great cerebral vein.

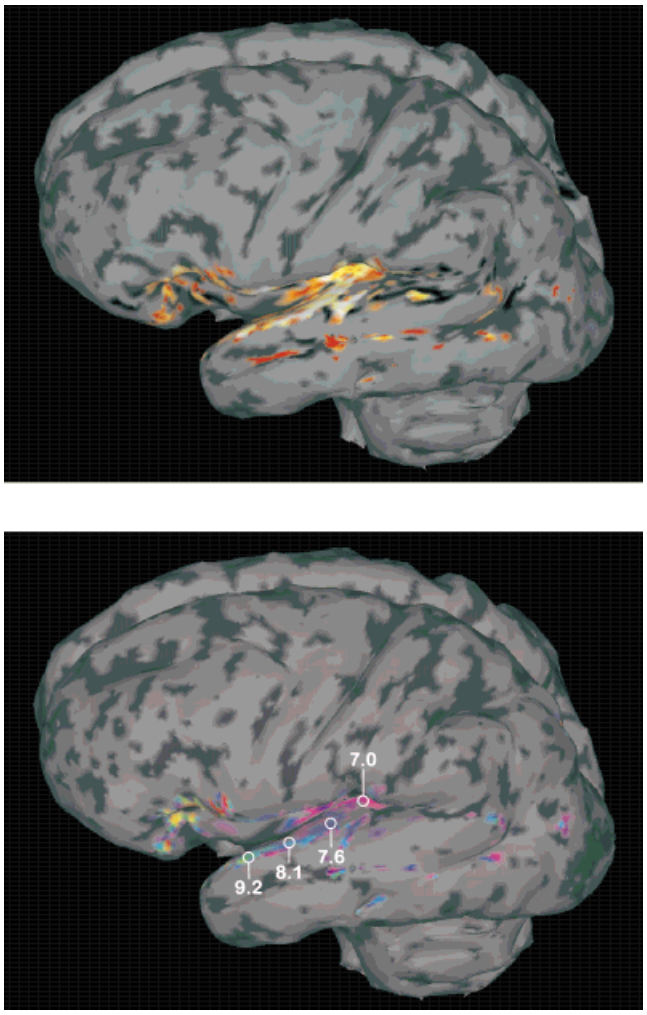

Figure 3.
Surface view of the left temporal lobe. In the top figure, z-scores are mapped onto the surface, in the lower figure, lag times (in s) are displayed. Four regions with averaged timings mark a signal trajectory along the superior temporal gyrus. Color coding of the z-scores and lag times correspond to Fig. 2.

In contrast to the results from behavioral data, there was a high overall dependency (i.e., over all activated regions) between the norm and the correctness manipulation: presentation of an incorrect sentence led to an increase of the lag (245 msec), the norm (17%), and the dispersion (100 msec). The training effect was found as a slight decrease of the lag (−360 msec), norm and dispersion were constant.

Next, we looked at individual regions and tested for interactions between the norm, the lag, and the dispersion with the sentence length and the correctness

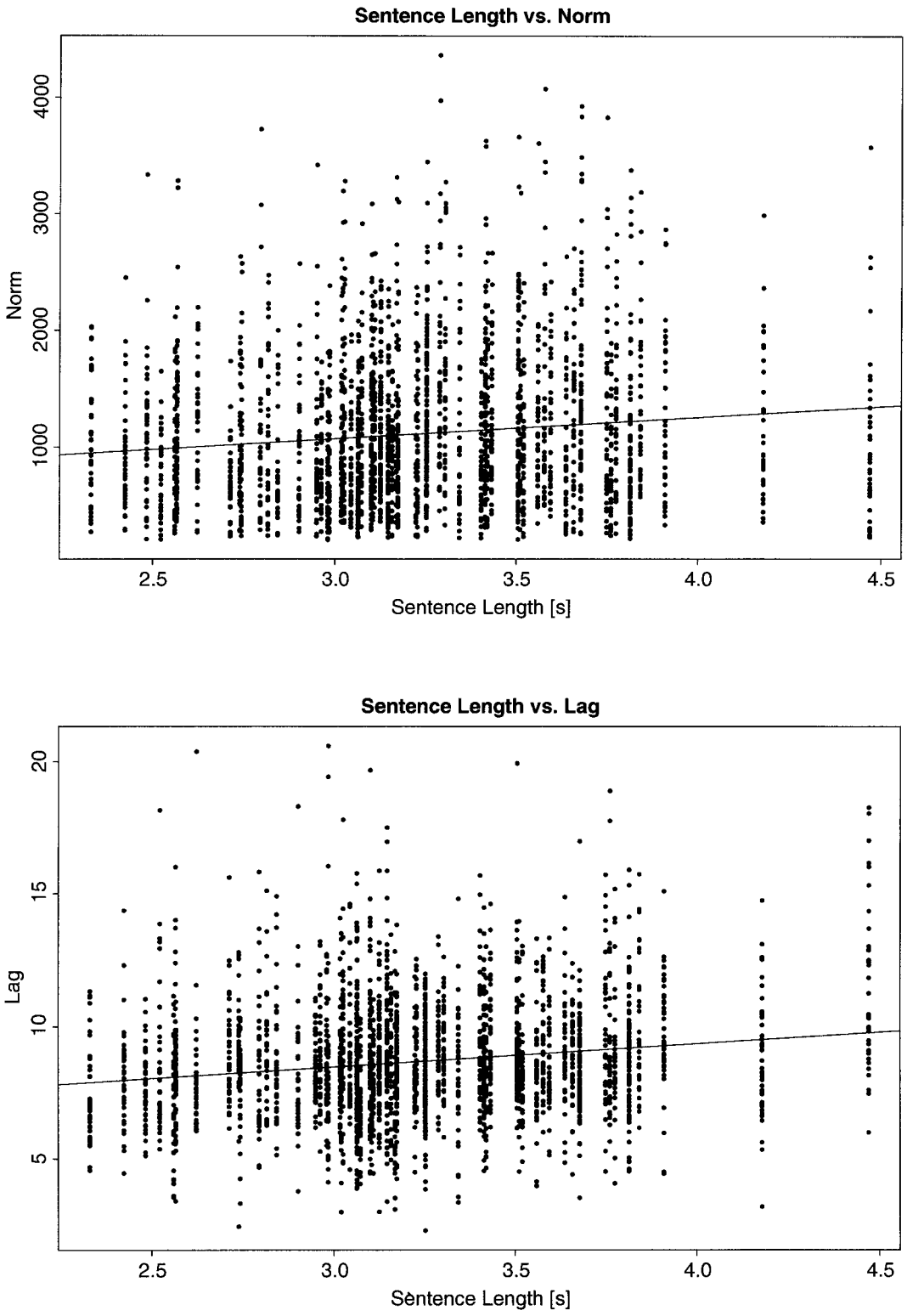

Figure 4.

Dependency of norm and lag on sentence length. Parameters of the regression lines are for the norm ($526 + 210x$, $R^2 = 0.014$, $p = 4e - 8$) and for the lag ($5.84 + 0.88x$, $R^2 = 0.027$, $p = 3e - 15$). A similar high correlation is found for the dispersion vs. the sentence length.

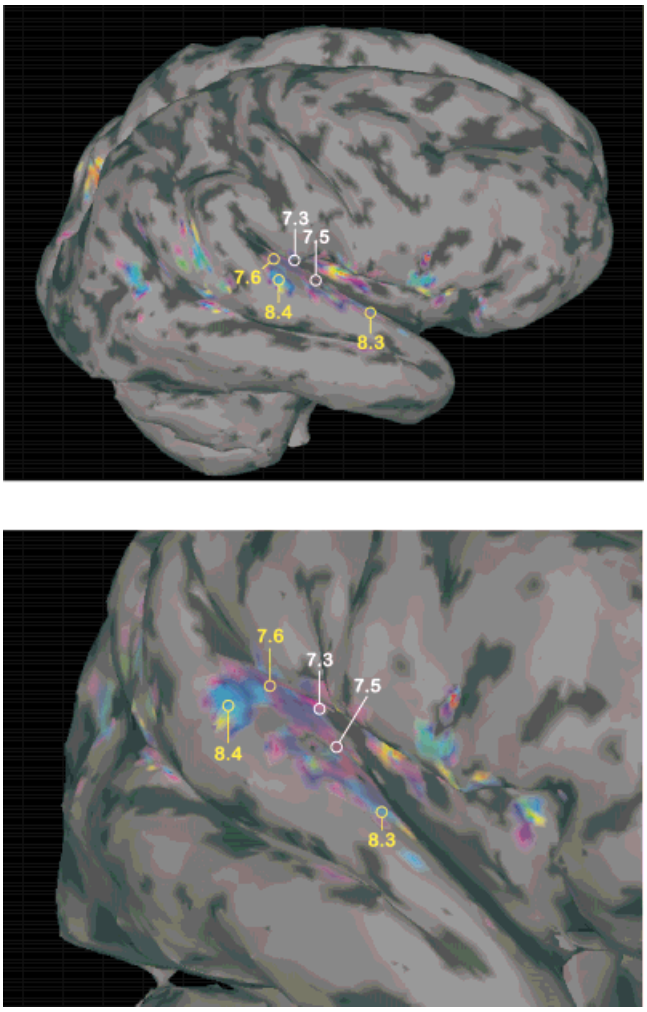

Figure 5.
Surface view of the right temporal lobe, showing average lag times for ROIs. Early responses are located in Heschl's gyrus, which only show a dependence on the sentence length (numbers in white). Middle responses, which are located more laterally and anteriorly, show a dependency on the correctness manipulation (numbers in green). Color coding of the z-scores and the lag values correspond to the scales in Fig. 2.

manipulation at the single trial level. Significant interactions ($P < 0.05$) between the norm and the sentence length were found in ROIs on the left superior temporal gyrus (see Fig. 3) as well as on the right side (see Fig. 5). The correctness manipulation interacted with the norm only in the left thalamus, the precuneus, and a few ROIs on the right superior temporal gyrus (Fig. 5). Interestingly, only "early" responses (white circles) interacted with the norm, "middle" responses (green circles) with the correctness manipulation.

We summarize from these results: (1) on the basis of an EPI protocol using a repetition time of 2 sec, lag time differences of ~250 msec were resolved in a series of 76 single trials, (2) we were able to show that the auditory cortex arose before secondary, language-related areas, then veins, (3) a temporal sequence of activated regions was found to originate from Heschl's gyrus and spread along the superior temporal gyrus anteriorly and laterally, and (4) it was possible to connect stimulation data (i.e., sentence length, responses) with estimated model parameters in a meaningful way.

Example group study

To underline further the usefulness of this approach, we re-evaluated a group of datasets acquired in a fMRI study of working memory [Zysset et al., 1998]. Subjects learned three sets of letters (4, 6, or 8 characters) at least 2 days before the scanning session. A trial started with the display of a small red box (for 800 msec), followed by the cue and after a delay (0, 2 or 4 sec), the probe. Subjects had to indicate by a button press whether the probe item belonged to the cued set, 108 randomized trials were run using an intertrial interval of 18 sec. Seven axial slices (64×64 voxels, $3.8 \times 3.8 \times 5$ mm voxel size, 2 mm gap) were recorded using an EPI protocol using a repetition time of 1 sec. All timings were corrected for the slice acquisition delay in the EPI protocol. Seven healthy female and six male students (age 22.3 ± 1.4 years) were included in the study; all finished the experiment. From an alphabetical list of coded filenames, we selected every third dataset ($n = 4$) for inclusion in this evaluation. We concentrated on six ROIs, which are shown in Figure 6.

We computed HR parameters (for each subject, trial, and ROI) and tested their dependency on the stimulation parameters. From the list of ROIs for a given subject, we selected those that most closely resemble the locations in Figure 6. The proper selection of a specific ROI from a larger cluster of activated voxels is critical: ROIs lateral to IPG_L (i.e., on the gyral crown) show different properties and may belong to a different functional area. Similar findings were made for ROIs superior and posterior to CMA, which presumably belong to the supplementary motor area and the precuneus. However, we consider an advantage of this method, that precisely corresponding anatomical regions are compared, without the need of using questionable intersubject alignment procedures.

Findings were summarized as follows: (1) all ROIs in all subjects show a significant increase of the lag values with increasing delay time, (2) in *CMA* and IPG_L, an increasing delay time leads to an increase of the dispersion, (3) only AI_L and PPC_L show a dependency

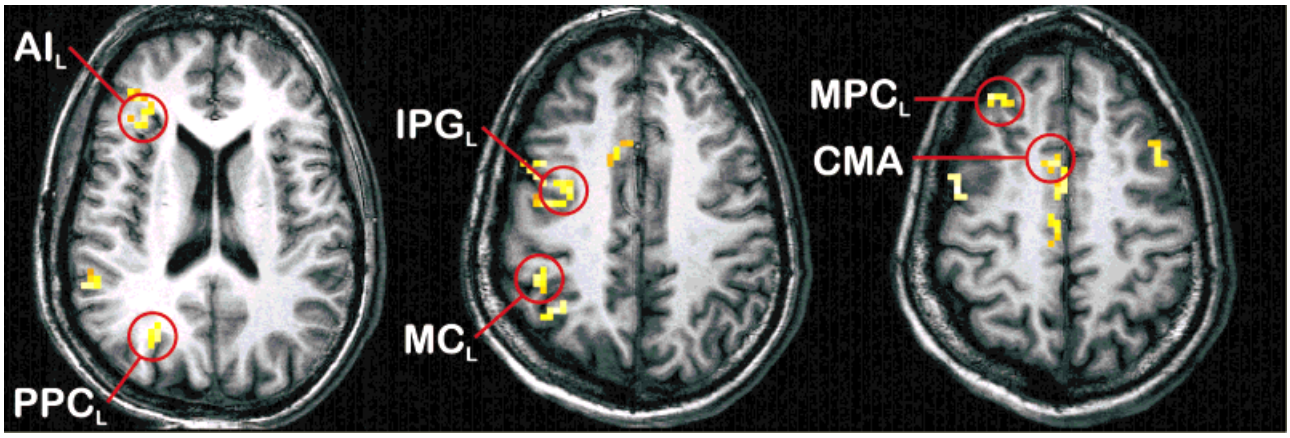

Figure 6.
ROIs in a working memory experiment: AI$_L$: superior anterior insula, MPC$_L$: middle prefrontal cortex, IPG$_L$: inferior precentral gyrus, CMA: cingulate motor area, MC$_L$: motor cortex, PPC$_L$: posterior parietal cortex.

of the norm on the set size, and (4) a slight decrease of the norm with the trial number (i.e., the experiment length) was found for most regions, but rarely reached significance. It is again interesting to note that an increase in the norm is found in conjunction with a higher ''computational burden,'' here the set size.

We studied the order and duration in which ROIs are activated. We defined the HR onset and outset times as the difference (resp. sum) of the lag and the dispersion. Sample results for a single subject, averaged within trials of the same delay time, are compiled in Table 2.

We found differences in the onset and outset times of up to 2 sec between subjects, which were much higher than the within-subject variances. This suggests use of the relative time to order in intrasubject comparisons instead of building group averages. We assigned this order by performing t-tests (paired within a trial, unequal variance, single-sided) between ROI timings. By comparison within the group, we could separate the ROIs into: (1) a group of ''early'' regions (CMA, AI_L) that are predominantly active during the first (encoding) phase of the experiment, (2) a ''middle'' group (IPG_L, MPC_L, PPC_L), which follows the first group in onset time and is active throughout the delay phase, and (3) a ''late'' group (MC_L), which is predominantly active during the response phase.

Discussion of results

By adapting a Gaussian model function to the HR, we extracted the shape-describing parameters norm, lag, and dispersion and studied the temporal properties of the HR. Our experiences with this approach are:

- On the basis of typical single-trial fMRI design, using a repetition time TR of 1 or 2s with 6–18 acquisitions per trial, it is possible and useful to model the HR in single trials and per ROI.
- Whereas the variance in lag times for single estimations was in the order of 600 msec, it was shown that in repeated measurements, temporal differences down to 250 ms (in experiment 1) and 100 msec (in experiment 2) could be resolved. This is close to the physical limit of $TR/\sqrt{n}$, where n the number of trials.
- Estimated parameters for the norm, lag, and dispersion varied with experimental manipulations and differed between subjects.
- We found an upper bound for the ratio of gain and dispersion (i.e., the slope) of the hemodynamic response: thus a very high norm required an increase in lag and dispersion. This upper bound depended on the activation site and the subject.

TABLE II. Onset and outset times (in sec after stimulus onset) of the HR vs. delay times in the ROIs of Figure 6

ROI	Onset			Outset		
delay [s]	0	2	4	0	2	4
CMA	2.27	2.53	2.92	8.41	8.62	9.48
AI_L	3.02	2.92	3.62	8.81	8.85	10.04
IPG_L	3.41	3.16	4.50	9.41	9.37	10.71
MPC_L	3.53	2.94	4.39	9.46	9.58	10.89
PPC_L	3.79	3.33	4.46	10.43	9.92	11.03
MC_L	4.06	4.25	5.73	10.44	10.89	12.29

- Homogeneously activated regions did not necessarily exhibit consistent temporal properties, i.e., they may span different functional cortices.
- Experimentally introduced response delays resulted in shifts in the lag. A longer stimulation induced a shift in the lag, and an increase in the dispersion. High correlations between the dispersion and stimulus duration were found (see Fig. 4).
- An experimentally introduced higher computational demand was reflected in a higher norm, but not generally in a longer duration of the HR.
- Norm and lag generally tended to decrease slightly with experiment duration, indicating training effects or habituation.
- A consistent relative ordering of activations by their onset and outset times in a group of subjects was found to be more informative than comparing group average times.

In the language comprehension experiment, a temporal sequence of activations was found, which spread from Heschl's gyrus to the lateral surface of the superior temporal gyrus and anteriorly to the tip of the temporal lobe. Differences in lag times found here correspond nicely with similar values obtained at comparable brain locations in a study of human auditory processing [Robson et al., 1998]. These locations may correspond to the recently described ''pitch processing areas'' [Griffith et al., 1998; Zatorre, 1998], which are assumed to take part in the analysis of temporal structures in sound.

The spatial activation pattern obtained in the working memory study compares nicely with a similar study of episodic memory [Buckner et al., 1998a]. Using a set of Gamma model function with fixed shape parameters but varying lag times, areas were separated into ''early,'' ''middle,'' and ''late'' responses for their temporal properties [Buckner et al., 1998b] and a temporal shift of the AI_L activation was found [Schacter et al., 1997]. Our procedure automatically adapts to shape and lag variations, and the corresponding HR parameters are directly derived from the data.

We must emphasize that the estimated HR parameters do not directly allow us to draw conclusions about the properties of the underlying neuronal activations. Some findings of this study, i.e., the shift of the lag with the experimental delay in the working memory experiment, are directly understandable in terms of the experimental context and thus will reflect time shifts of the activation pattern. An increase in the norm of the HR was consistently found with an increase of the ''computational burden,'' i.e., an increase of the set size in the memory experiment or the presentation of a grammatically incorrect sentence.

We doubt, however, that the estimated lag times correspond directly to the timescale of neuronal events: differences of lag times of >2 sec on the left superior temporal gyrus (see Fig. 3) are hard to explain by cognitive mechanisms alone. From fMRI data alone, we are unable to derive information whether the BOLD signal stems from capillary or venous compartment, which may explain differences in lag values of >1 sec. When comparing ROIs in distinct cortices, variations in the vascularization pattern and the vessel reagibility may influence the HR shape. It is not surprising that we find interindividual differences in lag and dispersion times of homologous cortical areas that are not directly reflected in the reaction times.

From the temporal activation pattern in the working memory experiment, we may also learn that several sites in the brain are simultaneously activated: even the BOLD signal in the motor cortex rises much before a response is required. Activations that last beyond the experimental response may reflect postprocessing (i.e., control processes).

Prerequisites for applying this statistical framework are: (1) a fMRI scanning protocol with a TR of 2 sec or better, (2) a trial length of at least 12 sec in order to collect and identify separate responses, (3) or at least six acquisitions per trial. Because a low signal-to-noise ratio implies a high variance of parameter estimates, it is advisable to apply this method to highly activated regions. Preprocessing for baseline correction and reduction of physiological and system noise [Kruggel et al., 1998] is helpful here.

GENERAL DISCUSSION

We consider the description of the HR by a model function a major advantage because it provides a compact and concise parameterization of the HR shape. Current choices for model function are arbitrary, since none is based on a comprehensive physiological model. The preference of the Gaussian function in this study is only justified by the fact that we obtained the best fits in a nonlinear estimation procedure. Deriving model functions from empirical studies is questionable. Because HR vary with experimental conditions, averaging over responses will introduce unpredictable shape changes in the mean response. High noise levels in the BOLD signal and only a few time points per period impede a clever selection of trials from the time course directly. We are aware of restrictions imposed by

choosing a Gaussian model function. Four problems should be mentioned:

1. The Gaussian function is symmetric. By visual inspection, we had the impression that early responses are asymmetric, i.e., the rising edge is steeper. Late responses (especially from venous areas) tend to be more symmetric.
2. We did not model the initial negative dip [Ernst and Hennig, 1994] and the terminal undershoot [Menon et al., 1993], which were demonstrated for BOLD signals from the visual cortex. By correcting for baseline fluctuations, we centered the signal and thus lost any information about a reference intensity. With the short trial periods of the experiments shown here, the undershoot is superimposed by the rising edge of the next response. In addition, it is still under discussion whether the initial dip is detectable in cortices other than V1.
3. If a Gaussian model function is understood as a result from a linear convolution, the underlying neuronal event should be infinitely short. Some stimuli (e.g., the aural presentation of a sentence) will elicit a neuronal activation that lasts for a few seconds. Thus the corresponding HR will only approximately be modeled by a Gaussian function.
4. We implicitly assumed that the response is monophasic, i.e., there is only one HR per trial. Multiphasic HRs are expected to be detected by the F-statistics as a high rate of misfits in a specific ROI. In the experiments of this study, we did not find clear examples of multiphasic HRs.

Some of these issues may be resolved by introducing more complex model functions. However, most of our current fMRI experiments are conducted with a preference of spatial resolution over temporal resolution, so that only 6–18 time points per period are available. This imposes limits for the amount of model parameters. The estimation context proposed here allows us to change model functions easily.

Whereas the HR estimation is performed in a nonlinear regression context, all subsequent statistical models to compare the HR parameters with behavioral variables and experimental conditions are multivariate linear regressions. If we plan to infer from HR parameters about properties of the underlying neuronal activations, we need to take care that linear relations among a stimulus, the neural response, and the HR may not hold. In recent studies of HR properties in event-related experimental designs, roughly linear properties of the hemodynamic response in terms of additivity in rapidly repeated single trials were demonstrated [Dale and Buckner, 1997]. However, it is well known from animal experiments that, e.g., the stimulus duration is not mapped linearly to a neuronal activation. Nonlinear activation properties have been demonstrated in the form of a ''u-shaped behaviour'' of the HR norm vs. the word stimulation frequency [Friston et al., 1998a] and for short (<6 sec) auditory stimuli [Robson et al., 1998] as well as short (<4 sec) visual stimuli [Vazquez and Noll, 1998a].

There were issues raised about the assumption that trials (and thus their HRs) are independent [Buckner et al., 1998a; Vasquez and Noll, 1998b]. If such influences exist, they must be taken into account either by randomization of the stimulation pattern, or included in the statistical model as a confound. We consider it a positive side effect of the analytical model proposed here, that the estimation context is separated from statistical models regarding the experimental manipulation. In the form of the HR parameter data sets, we obtain a very compact description of the experimental results, which may be followed by any suitable statistical inference.

The purpose of this report is twofold: (1) to show how the temporal information can be derived from the hemodynamic response in fMRI data, and (2) that it is possible to compare behavioral data with HR shape parameters in a meaningful way. By careful modification of the experimental context in an event-related setting, it is possible to draw conclusions from the HR shape about the underlying neuronal activation, assuming a linear convolution model. The time domain is another dimension available for experimental manipulation in fMRI experiments and thus another approach for investigating the dynamical properties of the brain.

ACKNOWLEDGMENTS

The authors thank C.J. Wiggins for providing the data sets, M. Meyer and S. Zysset for designing and conducting the fMRI experiments, and M. Pelegrini for suggestions on the manuscript.

REFERENCES

Bates D, Watts D. 1988. Nonlinear Regression Analysis and Its Applications. New York: Wiley-Liss, Inc.

Belliveau JW, Kennedy DN, McKinstry RC, Buchbinder BR, Weisskoff RM, Cohen MS, Vevea JM, Brady TJ, Rosen BR. 1991. Functional mapping of the human visual cortex by magnetic resonance imaging. Science 254:716–719.

Benali H, Buvat I, Anton JL, Pelegrini M, Di Paola M, Bittoun J, Burnod Y, Di Paola R. 1997. Space-time statistical model for functional MRI image sequences. In: Information Processing in Medical Imaging (LCNS 1230). Heidelberg: Springer.

Buckner R, Bandettini R, O'Craven K, Savoy R, Petersen S, Raichle M, Rosen B. 1996. Detection of transient and distributed cortical activation during averaged single trials of a cognitive task using functional magnetic resonance imaging. Proc Natl Acad Sci USA 93:14878–14883.

Buckner RL, Koutstaal W, Schacter DL, Wagner AD, Rosen BR. 1998. Functional-anatomic study of episodic retrieval using fMRI (I). Neuroimage 7:151–162.

Buckner RL, Koutstaal W, Schacter DL, Dale AM, Rotte R, Rosen BR. 1998. Functional-anatomic study of episodic retrieval using fMRI (II). Neuroimage 7:163–175.

Bullmore E, Brammer M, Williams SCR, Rabe-Hesketh S, Janoth N, David A, Mellers J, Howard R, Sham P. 1996. Statistical methods of estimation and inference for functional MR Image analysis. Magn Reson Med 35:261–277.

Christensen R. 1991. Linear Models for Multivariate, Time Series, and Spatial Data. Heidelberg: Springer.

Cohen MS. 1997. Parametric analysis of fMRI data using linear systems methods. Neuroimage 6:93–103.

Cox C, Ma G. 1995. Asymptotic confidence bands for generalized nonlinear regression models. Biometrics 51:142–150.

Cressie NAC. 1993. Statistics for Spatial Data. New York: Wiley-Liss, Inc.

Dale AM, Buckner RL. 1997. Selective averaging of rapidly presented individual trials using fMRI. Hum Brain Mapp 5:329–340.

Ernst T, Henning J. 1994. Observation of fast response in functional MR. Magn Reson Med 32:146–149.

Friston KJ, Holmes AP, Worsley KJ, Poline JB, Williams CR, Frackowiak RSJ. 1994. Analysis of functional MRI time-series. Hum Brain Mapp 1:153–171.

Friston KJ, Worsley KJ, Frackowiak RSJ, Mazziotta JC, Evans AC. 1994. Assessing the significance of focal activations using their spatial extent. Hum Brain Mapp 1:210–220.

Friston KJ, Fletcher P, Josephs O, Holmes A, Rugg MD, Turner R. 1998. Event-related fMRI: characterizing differential responses. Neuroimage 7:30–40.

Friston KJ, Josephs O, Rees G, Turner R. 1998. Nonlinear event-related responses in fMRI. Magn Reson Med 39:41–52.

Gjedde A. 1997. The relation between brain function and cerebral blood flow and metabolism. In: Cerebrovascular Disease. Philadelphia: Lippincott-Raven.

Griffith TD, Büchel C, Frackowiak RSJ, Patterson RD. 1998. Analysis of temporal structure in sound by the human brain. Nat Neurosci 1:422–427.

Hartley HO. 1964. Exact confidence regions for the parameters in nonlinear regression laws. Biometrika 51:347–353.

Josephs O, Turner R, Friston KJ. 1997. Event-related fMRI. Hum Brain Mapp 5:243–248.

Kim SG, Richter W, Ugurbil K. 1997. Limitations of temporal resolution in functional MRI. Magn Reson Med 37:631–636.

Kruggel F, Descombes X, von Cramon DY. 1998. Preprocessing of fMRI datasets. In: Workshop on Biomedical Image Analysis (Santa Barbara), Los Alamitos: IEEE Computer Press, pp 211–220.

Kruggel F, von Cramon DY. 1999. Modeling the hemodynamic response in single trial fMRI experiments. Magn Reson Med (in press).

Kwong KK, Belliveau JW, Chesler DA, Goldberg IE, Kennedy DN, Weisskoff RM, Poncelet BP, Hoppel BE, Cohen MS, Turner R, Cheng H, Brady TJ, Rosen BR. 1992. Dynamic magnetic resonance imaging of the human brain activity during sensory stimulation. Proc Natl Acad Sci USA 89:5675–5679.

Lange N, Zeger SL. 1997. Nonlinear Fourier time series analysis for human brain mapping by functional magnetic resonance imaging. J Roy Stat Soc Appl Stat 46:1–29.

Lee AT, Glover GH, Meyer CH. 1995. Distribution of large venous vessels in time-course spiral blood-oxygen-level-dependent magnetic resonance functional neuroimaging. Magn Reson Med 33:601-745–754.

Luknowsky DC, Thomas CG, Gati JS, Menon RS. 1998. Millisecond sequencing of neural activation in simple tasks determined by the BOLD fMRI neurovascular response. Neuroimage 6:S280.

Menon RS, Ogawa S, Tank DW, Ugurbil K. 1993. 4 Tesla gradient recalled echo characteristics of photic stimulation-induced signal changes in the human primary visual cortex. Magn Reson Med 30:380–386.

Meyer M, Friederici AD, von Cramon DY, Kruggel F, Wiggins CJ. 1998. Auditory sentence comprehension: different BOLD patterns modulated by task demands as revealed by a 'single trial' fMRI study. Neuroimage 7:S181.

Neumaier A, Schneider T. 1998. Multivariate autoregressive and Ornstein-Uhlenbeck processes: estimates for order, parameters, spectral information, and confidence regions. http://www.aos.princeton.edu/WWWPUBLIC/tapio/papers/arfit.html

Ogawa S, Tank DW, Menon R, Ellermann JM, Kim SG, Merkle H, Ugurbil K. 1992. Intrinsic signal changes accompanying sensory stimulation: functional brain mapping with magnetic resonance imaging. Proc Natl Acad Sci USA 89:5951–5955.

Piepgras U. 1977. Neuroradiologie. Stuttgart, Thieme.

Press WH, Flannery BP, Teukolsky SA, Vetterling WT. 1992. Numerical recipes in C. Cambridge: Cambridge University Press.

Rajapakse JC, Kruggel F, von Cramon DY. 1998. Modeling hemodynamic response for analysis of functional MRI time-series. Hum Brain Mapp 6:283–300.

Robson MD, Dorosz JL, Gore JC. 1998. Measurements of the temporal fMRI response of the human auditory cortex to trains of tones. Neuroimage 7:185–198.

Schacter DL, Buckner RL, Koutstaal W, Dale AM, Rosen BR. 1997. Late onset of anterior prefrontal activity during true and false recognition: an event-related fMRI study. Neuroimage 6:259–269.

Seber GAF, Wild CG. 1989. Nonlinear Regression. New York: Wiley-Liss, Inc.

Singh M, Kim T, Khosla D. 1995. Separation of veins from activated brain tissue in functional magnetic resonance images at 1.5T. IEEE Trans Nucl Sci 42:1338–1341.

Sorensen JA, Wang X. 1996. Problems in estimating hemodynamic response parameters from fMRI data. Hum Brain Mapp 4:265–272.

Vazquez AL, Noll DC. 1998. Nonlinear aspects of the BOLD response in functional MRI. Neuroimage 7:108–118.

Vazquez AL, Noll DC. 1998. Time-invariant properties of the BOLD response. Neuroimage 7:S579.

Vilringer A, Dirnagl U. 1995. Coupling of brain activity and cerebral blood flow: basis of functional neuroimaging. Cerebr Brain Metab Rev 7:240–276.

Walter E, Ponzatto L. 1997. Identification of Parametric Models. Heidelberg: Springer.

Zarahn E, Aguirre G, D'Esposito M. 1997. A trial-based experimental design for fMRI. Neuroimage 6:122–138.

Zatorre R. 1998. How do our brains analyze temporal structure in sound? Nat Neurosci 1:343–345.

Zysset S, Pollmann S, von Cramon DY, Wiggins CJ. 1998. Retrieval from long term memory and working memory. In: Cognitive Neuroscience Society: 1998 Annual Meeting Abstract Program. Harvard: MIT Press, p 83.